Heliyon 10 (2024) e36048

Contents lists available at ScienceDirect

Heliyon

journal homepage: www.cell.com/heliyon

Research article

Exploring the uncharted seas: Metabolite profiling unleashes the anticancer properties of *Oscillatoria salina*

Bornita Das [a,1], Asharani Prusty [a,b,1], Subhajeet Dutta [a,b], Aditi Maulik [a], Yogita Dahat [b,c], Deepak Kumar [b,c], Sucheta Tripathy [a,b,*]

[a] *Computational Genomics Lab, Structural Biology and Bioinformatics Division, CSIR Indian Institute of Chemical Biology, 4, Raja S.C. Mullick Road, Kolkata, 700032, India*
[b] *Academy of Scientific and Innovative Research (AcSIR), Ghaziabad, 201002, India*
[c] *Organic and Medicinal Chemistry Division, CSIR Indian Institute of Chemical Biology, 4, Raja S.C. Mullick Road, Kolkata, 700032, India*

ARTICLE INFO

Keywords:
Marine cyanobacteria
Oscillatoria salina, A549 cells
Apoptosis
Cytoskeleton
Rap1

ABSTRACT

Marine cyanobacteria offer a rich source of varied natural products with both chemical and biological diversity. *Oscillatoria salina* (*O. salina*) is a filamentous non-heterocystous marine cyanobacterium from Oscillatoriaceae family. In this investigation, we have unveiled bioactive extracts from *O. salina* using two distinct solvent systems, revealing significant anticancer properties. Our assessment of the organic and aqueous extracts (MCE and AE) of *O. salina* demonstrated pronounced antiproliferative and antimetastatic effects. Notably, this study is the first to elucidate the anticancer and anti-metastatic potential of *O. salina* extracts in both 2D and 3D cell culture models. Both MCE and AE induced apoptosis, hindered cell proliferation, invasion, and migration in A549 non-small cell lung cancer cells, accompanied by alterations in cell morphology and cytoskeleton collapse. Moreover, MCE and AE induced spheroid disintegration in A549 cells. Transcriptomics analysis highlighted the significant involvement of Rap1 and p53 signaling pathways in mediating the observed antitumor effects. Mass spectroscopy characterization of these extracts identified 11 compounds, some known for their anticancer potential. HPLC analysis of AE revealed six peaks with UV absorption spectra resembling phycocyanin, a cyanobacterial pigment with well-known anticancer activity. Collectively, these findings underscore the anticancer potential of MCE and AE, containing bioactive metabolites with anticancer and antimetastatic properties.

1. Introduction

The ocean harbors a vast collection of marine species containing valuable natural pharmaceutical compounds with significant potential. In recent times a heightened interest on the production of bioactive metabolites from marine organism has surfaced [1]. This is propelled by a mounting body of literature showcasing the beneficial effects of these compounds on human health. Numerous marine organisms, particularly those lacking robust physical defenses like shells or spines, have developed chemical weaponry for defensive or

* Corresponding author. Computational Genomics Lab, Structural Biology and Bioinformatics Division, CSIR Indian Institute of Chemical Biology, 4, Raja S.C. Mullick Road, Kolkata, 700032, India.
E-mail addresses: tsucheta@iicb.res.in, tsucheta@hotmail.com (S. Tripathy).
[1] Equal contributors.

https://doi.org/10.1016/j.heliyon.2024.e36048
Received 9 April 2024; Received in revised form 7 August 2024; Accepted 8 August 2024
Available online 10 August 2024

competitive advantages. Remarkably, certain lesser-known bioactive substances with therapeutic potential emerge from these chemical arsenals. Filamentous cyanobacteria hold a unique position among marine organisms and captivate the attention of chemists due to their ability to produce plethora of bioactive molecules. Over 1600 distinct molecules originating from cyanobacteria have been identified and categorized into 260 metabolite families. Among these families, 148, which constitute 53 % of the total, are associated with marine environments [2]. Their extensive structural variability arises from their capacity to combine non-ribosomal peptide synthetases with polyketide synthases, alongside various enzymes responsible for various biosynthetic conversions. This combination resulted in a broad range of chemically diverse natural products, including but not limited to glycolipids, macrolides, peptides (including depsipeptides and lipopeptides), and polyketides [3–7].

Secondary metabolites sourced from cyanobacteria have attracted much scientific attention owing to their demonstrated cytotoxic effects on various cancer cell lines. Among the 260 reported families of metabolites, a substantial 42 % amounting to up to 110 families have exhibited cytotoxic properties [2]. Presently, numerous therapeutic agents, either directly derived from cyanobacteria or inspired by them, are undergoing clinical trials. A significant proportion of the studied and documented cytotoxic secondary metabolites originating from marine cyanobacteria are primarily associated with two specific orders: Oscillatoriales and Synechococcales. In terms of cytotoxic metabolite production, cyanobacteria belonging to the order Oscillatoriales stand out as one of the most prolific groups [8].

Oscillatoria salina (O. salina) is a marine filamentous cyanobacteria belonging to the Oscillatoriaceae family. Our laboratory pioneered the genome sequencing of this strain of cyanobacteria using both Illumina and Oxford Nanopore platform. Genome analysis of *O. salina* hinted at the presence of certain metabolites with anticancer properties. This strain of cyanobacteria can be cultured and harvested easily in laboratory condition facilitating an environmentally friendly strategy for drug discovery to address challenges associated with the excessive exploitation of marine resources. While numerous studies have explored the anticancer properties of different cyanobacterial metabolites, the investigation of the anticancer activity of *O. salina* remains elusive.

Cancer remains a leading cause of mortality worldwide, claiming approximately 10 million lives in 2020. Despite advancements in cancer therapies, the battle against this disease faces significant hurdles, including drug resistance, lack of selectivity towards specific emerging cancers, and severe side effects [9,10]. Amidst these challenges, marine cyanobacteria have emerged as a promising source of anticancer agents, offering a treasure trove of compounds with potent antiproliferative and apoptotic activities against various cancer cell lines.

Over their 2.8 billion years of evolution, cyanobacteria have developed the remarkable ability to synthesize a vast array of bioactive molecules due to their adaptation to numerous environmental stresses. These molecules exhibit cytotoxic properties that can be harnessed as powerful anticancer agents. They primarily function by disrupting cellular signaling pathways, inducing apoptosis, causing mitochondrial dysfunction, arresting the cell cycle, and generating oxidative stress. Notable cyanobacterial metabolites, such as dolastatin, somocystinamide A, lyngbyabellin, malyngolide, curacin A, and kalkitoxin, have demonstrated significant anticancer activities in various cell lines through diverse mechanisms of action [11].

In our study, we explored the anticancer properties of organic (1:1 methanol-chloroform) and aqueous extracts (AE) from a previously unstudied strain of cyanobacteria, *O. salina*, in human lung adenocarcinoma A549 and human ovarian cancer SKOV-3 cells. Both MCE and AE showed dose dependent cytotoxicity in A549 and SKOV-3 cells. In addition, AE and MCE also exhibited substantial anticancer potential in a 3D spheroid model formed by A549 cells, while SKOV-3 spheroids remained unaffected by these extracts. Our research also delved into the mechanistic pathways underlying the anticancer properties of *O. salina* extracts. Furthermore, we sought to identify the bioactive components present in both the aqueous and organic extracts using advanced techniques such as mass spectrometry, HPLC, IR, and NMR spectroscopy. This study highlights the immense potential of *O. salina* as a source of novel anticancer agents, paving the way for future therapeutic developments.

2. Materials and methods

2.1. Culture and maintenance of cyanobacteria

The *O. salina* culture was obtained from the National Facility for Marine Cyanobacteria (NFMC) at Bharathidasan University in Tamilnadu, India (accession number: BDU10142). The organism was cultured in ASN III media at a pH level of 7.5. The culture was nurtured inside an incubator shaker set at a temperature of 25 °C, and the shaking speed was maintained at 130 rpm. The incubator was equipped with a lighting system that provided an intensity of 3000 lux, following a 16 h light and 8 h dark photoperiod cycle. To ensure the culture's vitality, sub-culturing with ASN III media was done every 30 days. The organism's morphology was periodically examined using an EVOS XL inverted light microscope.

2.2. Extraction of metabolites from cyanobacteria

To extract metabolites, biomass was regularly harvested from 30-day-old cultures of *O. salina*. The biomass was washed thrice with autoclaved water and was subsequently subjected to lyophilization under reduced pressure.

To prepare 1:1 methanol: chloroform extract (MCE), 1 g of the lyophilized material was re-suspended in a 30 ml mixture of methanol and chloroform in equal proportions. This suspension was then subjected to bath sonication for 30 min. The resulting extract was filtered through Whatman filter paper grade 1. This entire extraction process was repeated five times. After extraction, the solvent was removed from the extract using a rotary evaporator. Any remaining traces of solvent were eliminated by freeze-drying the extract under reduced pressure.

To prepare the aqueous extract (AE) 0.5 g of lyophilized biomass was mixed with 30 ml of autoclaved water and vortexed. The sample was subjected to three freeze thaw cycles (freezing at −20 °C for 2 h followed by thawing at ambient temperature for 1 h). The supernatant was then filtered and subjected to lyophilization that resulted in a blue powder containing water soluble metabolites.

2.3. Cell culture and treatment

The A549, SKOV-3 and HEK-293 (normal human embryonic kidney cell) cells were procured from NCCS, Pune. A549 and SKOV-3 cells were cultured in RPMI-1640 medium sourced from Gibco, USA and HEK-293 was cultured in DMEM sourced from Gibco, USA. All medium was further enriched with 10 % heat-inactivated fetal bovine serum (FBS) (Gibco, USA), and supplemented with penicillin-streptomycin (Gibco, USA). The cells were cultured in a controlled environment at 37 °C, with a humidified atmosphere containing 5 % CO_2.

For MCE treatment, measured quantity of lyophilized MCE was dissolved in 2 % dimethyl sulfoxide (DMSO) to prepare the stock solution. Subsequent working stocks were diluted in cell culture media. For every experiment, corresponding vehicle control was taken. For AE treatment, lyophilized AE was dissolved in autoclaved water to prepare the stock and subsequent working solutions were prepared by diluting with cell culture media.

2.4. Study of cytotoxicity by MTT assay

The cytotoxicity induced by MCE and AE of *O. salina* in A549, SKOV-3 and HEK293 cells was determined by MTT [3-(4,5-dimethylthiazol-2-yl)-2,5-diphenyltetrazolium bromide] assay. Briefly, the cells were seeded in a 96 well plate at a density of 8000 cells/well and incubated overnight. Then the cells were treated with different concentrations (10, 20, 50, 100 μg/ml) of MCE or AE of *O. salina* IICB1 and incubated for 24 h. After the treatment 50 μl of MTT solution (1.2 g/ml) was added in each well and incubated for 4 h. The resulting formazan product was dissolved in dimethyl sulphoxide and absorbance of the resulting solution was measured at 550 nm using a microplate reader. The percent cytotoxicity was calculated using the following formula: % cytotoxicity = $[1- (A_{test}/A_{control})] \times 100$, where A_{test} and $A_{control}$ are the absorbance of the test sample and control sample respectively.

2.5. Study of cell morphology

To investigate the alterations in morphology resulting from the treatment of MCE and AE of *O. salina*, cells were initially cultured in 35 mm culture dishes and were incubated overnight. Subsequently, the cells were exposed to different concentrations of MCE or AE. The distinct morphological changes in the treated cells were observed at various time intervals (48 h or 72 h) using EVOS cell imaging system (Life Technologies Corporation, Bothell).

2.6. Spheroid formation assay

A549 and SKOV-3 cells were seeded into Ultralow Adherence plates (Corning Inc., NY, USA) at a density of 10,000 cells per well and cultured in serum-free medium 3dGRO™ Spheroid Medium (Sigma, USA). The tumor spheres were allowed to grow for 7 days. After the formation of tumor spheres different concentrations of MCE or AE (10, 20 μg/ml) was added to each well and incubated for different time points (48 h or 72 h). After the treatment, the images of tumorsphere formation were taken in a microscope (Nikon, Japan).

2.7. Immuno-cytochemistry staining for cytokeratin-18 (CK-18) and F-actin

A549 cells were seeded and grown on coverslips to 70 % confluency. For CK-18 staining the cells were treated with MCE (10 μg/ml) or AE (10 μg/ml) and incubated for 24 h. For actin staining cells were incubated with MCE (10 μg/ml) or AE (10 μg/ml) for 48 and 24 h respectively. After treatment, cells were washed with 1X PBS and fixed with methanol (for CK-18) or 3.7 % formaldehyde (for F-actin) and permeabilized with acetone. The non-specific sites were blocked with BSA in PBS. For CK-18 staining, the cells were immune-labeled with CK-18 mouse monoclonal antibody (Cell Signaling Technology, USA, Catalogue No. 4548T) for 24 h and then incubated with FITC conjugated goat anti-mouse secondary antibody (Invitrogen, USA, Catalogue No. F2761) for 1.5 h at room temperature. For F-actin staining, the cells were incubated with Alexa Fluor 568 conjugated phalloidin (Invitrogen, USA, Catalogue No. A12380) solution for 1 h. The nucleus was counterstained with DAPI. The coverslips were finally mounted on glass slides and the images were taken in a Leica fluorescence microscope. All the experiments were performed in three independent replicates.

2.8. In-vitro wound healing assay

Wound-healing assay was done to assess the effect of MCE and AE of *O. salina* on migration of epithelial cells. The assay was carried out according to a previously published protocol [12] with slight modifications. Briefly, the cell monolayer in MCE or AE treated (2.5 μg/ml and 5 μg/ml) and untreated cells were scratched uniformly with the tip of a sterile pipette. The petridish containing the cells were rinsed with PBS to eliminate cell debris. Fresh serum free media was added and the wound closure was monitored and photographed at 0 and 24 h using an inverted microscope and camera (Nikon, Tokyo, Japan). Quantification of the percentage wound closure was done with ImageJ software using the following formula [13]:

Wound closure percentage = $(A_{t\ =\ 0} - A_{t=\ \Delta t})/A_{t\ =\ 0}$ X 100

2.9. Cell invasion assay

Cell invasion assay was done utilizing cell invasion assay kit (Millipore, MA, USA Catalogue No. ECM550) according to the manufacture's protocol. Cells grown in 60 mm dishes were treated with 10 and 20 μg/ml of either MCE or AE or their respective vehicle control for 24 h. After treatment, a cell suspension containing 0.5 X 10^5 cells/ml was prepared in serum free media. 300 μl of the cell suspension was placed on the upper chamber of the transwell insert and 500 μl of cell culture media containing 10 % FBS as chemo-attractant was added to the lower chamber and incubated for 24 h. After incubation, non-invading cells were removed from the interior of the inserts and the invading cells on the membrane were stained with the staining dye provided with the kit. The membrane was photographed using inverted microscope. The invaded cells were quantified by dissolving the stained cells in 10 % acetic acid and recording the OD at 560 nm.

2.10. Detection of apoptosis by flow cytometry

MCE and AE-induced apoptosis in A549 cells was evaluated using Annexin V –FITC Early Apoptosis Detection Kit (Cell Signaling Technology, MA, USA Catalogue no. #6592) following manufacturer's protocol. Briefly after treatment, cells were washed with ice cold PBS and re-suspended at a density of 10^6 cells/ml with 1X Annexin V binding buffer. 96 μl of the cell suspension was taken in an assay tube and 1 μl of Annexin V FITC conjugate and 12.5 μl of Propidium Iodide (PI) solution were added. The cell suspension was incubated on ice in dark for 10 min. After incubation it was diluted to a final volume of 250 μl with 1X Annexin V binding buffer and analyzed using FACS Calibur analyzer (BD Biosciences). All the tests were performed in three independent replicates.

2.11. Detection of cell proliferation by BrdU assay

MCE and AE-induced inhibition of cell proliferation was evaluated using BrdU Cell Proliferation Assay Kit (Cell Signaling Technology, MA, USA, Catalogue No. ≠6813) following manufacturer's protocol. Briefly, cells were seeded at a density of 5000 cells/well in a 96-well plate (Becton Dickinson, USA). After 24 h incubation, cells were treated with 10, 20, 50 and 100 μg/ml of MCE or AE for 24 h. Thereafter, cells were incubated with 10 X BrdU solution for 2.5 h followed by addition of fixing solution and incubation for 30 min. After the incubation period 1X BrdU detection antibody and 1X HRP-conjugated secondary antibody was added sequentially. Finally, TMB substrate was added and color change of the solution was observed. After the development of color the reaction was stopped using stop solution and the absorbance was read at 450 nm.

2.12. RNA isolation and quality checking

For transcriptome analysis cells were seeded in a 60 mm dish and grown to 70 % confluency. The cells were treated with 10 μg/ml MCE for 24 h or 10 μg/ml AE for 8 h. After treatment, the cells were washed with 1X PBS and total RNA was isolated using NucleoSpin RNA isolation kit (Macherey-Nagel, Germany) according to manufacturer's protocol. The quality of the isolated RNA was checked by 1 % agarose gel electrophoresis. Concentrations of RNA were measured with the NanoDrop ND-100 Spectrophotometer (NanoDrop Technologies, Wilmington, DE), and Qubit 4 Fluorometer (Thermo Fisher Scientific, USA) while RNA quality was assessed with the Tapestation 4200TM (Agilent Technologies, Santa Clara, USA). Samples which had a RIN value greater than 9 and 28S:18S rRNA ratio close to 2:1 was considered for transcriptome sequencing.

2.13. RNA-sequencing and bioinformatics analysis

For library preparation, RNA samples were taken with an initial RNA input of 500 ng "KAPA mRNA Capture kit" was used for mRNA capture by oligomag beads, followed by mRNA fragmentation using heat and magnesium. Next, the cDNA was synthesized using Reverse transcriptase and random hexamers. Prepared libraries were sequenced on Illumina Nextseq 2K to generate 35M, 2x150 bp reads/sample. Up to 75 % of the sequenced bases were of Q30 value > 90.

FASTQ files were generated using sequenced data. The raw reads were subjected to adapter trimming using BBDuk v38.87 [14]. The quality of the reads was estimated using FastQC v0.11.7 [15]. The high quality clean reads were processed through Snakemake pipeline v5.2.4 (https://github.com/computational-genomics-lab/RNAseq_read_summerization_pipeline-for-Eukaryotic-dataset) where alignment to the human genome was done using STAR v2.7.6a [16]. The human genome sequence Release 43 (GRCh38.p13) and gene annotation were downloaded from the GENCODE website. FeatureCounts v2.0.1 [17] was also used in the Snakemake pipeline to count the number of reads mapped to genomic features. Normalization and differential expression analysis were done using DESeq2 v1.34.0 in Galaxy v22.01 hosted in our local server (Supplementary file 3 and 4). Differentially expressed genes (DEGs) with P value < 0.05 and the log2fold change values with the cutoff of above 1.0 and below −1.0 were considered as upregulated and downregulated respectively. The selected sets of DEGs were subjected to functional annotation and Kyoto Encyclopedia of Genes and Genomes (KEGG) pathway analysis using the DAVID (Database for Annotation, Visualization, and Integrated Discovery)

bioinformatics tool [18,19].

2.14. Mass spectral analysis

1 mg of MCE was dissolved in methanol and 30 µl of solution was subjected to LC-MS/MS analysis utilizing an LTQ-Orbitrap Mass Spectrometer (Thermo Fisher Scientific, USA) equipped with a C18 hypersil gold column. Elution rate was kept at 0.300 ml/min using eluents A and B. Eluent A was 0.1 % formic acid in water, while eluent B was 0.1 % formic acid in acetonitrile. The run time was total 30 min.

2.15. HPLC analysis

HPLC analysis was performed with 5 mg/ml AE and 10 mg/ml MCE using Supelco Ascentis C18 (25 cm × 4.6 mm, 5 µm) column and mobile phase consisting of A: water (0.1 % v/v formic acid) and B: Acetonitrile (70:30 v/v 0–1 min; 5:95 v/v 1–21 min; 5:95 v/v 21–24 min; 70:30 v/v 24–25 min; 70:30 25–30 min) at a flow rate of 1 ml/min. The eluent was monitored at 620 nm and column temperature was maintained at ambient temperature.

2.15.1. 1 H NMR and IR analysis

^{1}H NMR spectra of extract is recorded on Bruker 600 MHz NMR using D_2O as solvent. IR spectrum of extract is recorded on Bruker Tensor-27 equipped with Opus software with ATR mode of analysis.

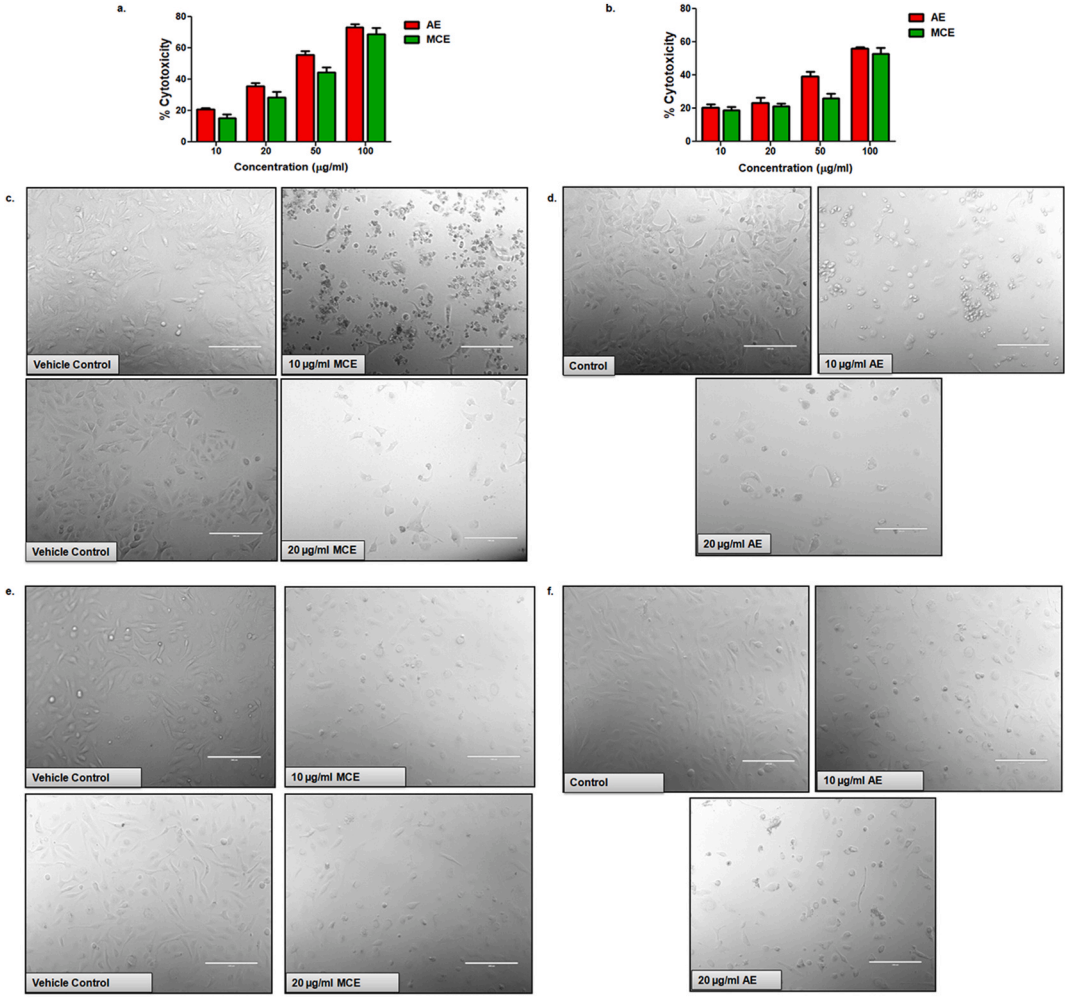

Fig. 1. Cytotoxicity and morphology change induced by *O. salina* extracts. a) and b) Cytotoxicity induced by MCE (10, 20, 50 and 100 µg/ml) and AE (10, 20, 50 and 100 µg/ml) in A549 and SKOV-3 cells respectively. c) and d) Alteration of cell morphology induced by 10 and 20 µg/ml of MCE and AE in A549 cells for 48 h and 24 h respectively, e) and f) Alteration of cell morphology induced by 10 and 20 µg/ml of MCE and AE in SKOV-3 cells for 48 h and 24 h respectively.

2.16. Statistical analysis

The statistical analyses were done using Prism v5.0 software unless otherwise stated. All the quantitative data were reported as mean ± SD obtained from at least three independent experiments. Comparisons between the two groups of samples were conducted using unpaired Student's t-test. Statistical significance was attributed to p-values below the threshold of 0.05.

3. Results

3.1. MCE and AE of O. salina induced cytotoxicity and changed the cell morphology in A549 and SKOV-3 cell lines

The marine cyanobacteria constitute a reservoir of biologically active secondary metabolites that has garnered scientific interest for their cytotoxic effects on various cancer cell lines [6]. In-silico analysis revealed that the *O. salina* genome harbors biosynthetic gene clusters coding for certain anticancer compounds (data unpublished). Here we aimed to see if the in-silico results are translatable into actual metabolites. To check the cytotoxic effect of AE and MCE, we performed MTT assay with MCE and AE in two different cancer cell lines: human lung adenocarcinoma cell line A549, human ovarian cancer cell line SKOV-3 and also in one normal human embryonic kidney cell line, HEK293. Both A549 and SKOV-3 showed dose dependent cytotoxic response to MCE and AE treatment (Fig. 1 a, b). The IC50 value was found to be 58.76 μg/ml and 66.05 μg/ml in A549 cells treated with AE and MCE respectively. For SKOV-3 cell line the IC50 was found to be 79.03 μg/ml and 90.448 μg/ml for AE and MCE treated cells respectively. Notably both AE and MCE elicited minimal cytotoxicity of 2.003 % and 4. 90 % at a concentration of 10 and 20 μg/ml respectively in HEK-293 cells (Supplementary Fig. 1 a, b).

To address the effects of MCE and AE of *O. salina* on these two cell lines, we confirmed the phenotypic experiments on these cells. The phenotypic change was more pronounced with AE treated A549 and SKOV-3 cells. Both A549 and SKOV-3 cells showed noticeable apoptotic morphologic changes including shrunk cell shape due to loss of adherent property with neighboring cells and to the surface, cell detachment and also diminished cell–cell junction as compared to normal epithelial morphology in control cells after 24 h of AE treatment. The same change in morphology was observed for MCE treated cells after 48 h of treatment for both the cell lines (Fig. 1 c, d, e and f). However, HEK293 cells showed no morphology change even after 48 h of MCE or AE treatment (Supplementary Fig. 1 c, d)

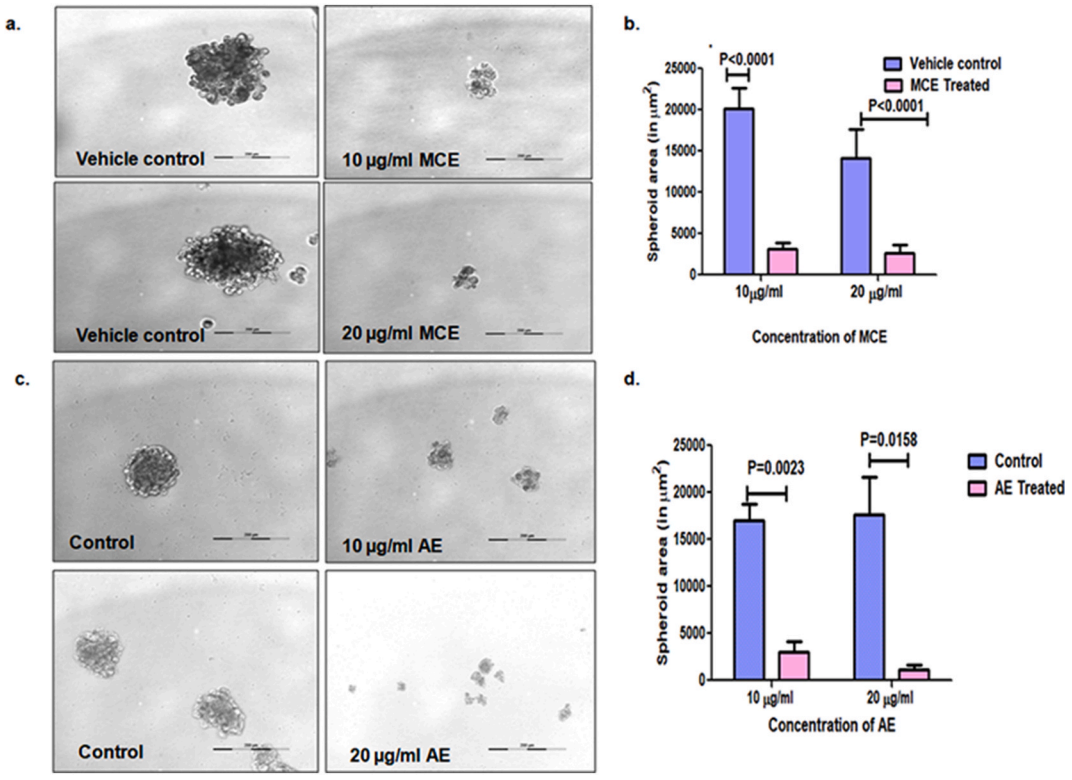

Fig. 2. Effect of *O. salina* extracts on spheroid formation in A549 cells. a) Representative image of the spheroids treated with 10, 20 μg/ml of MCE for 72 h, b) Graphical representation of the decrease in A549 spheroid area when treated with 10 and 20 μg/ml of MCE for 72 h, c) Representative image of the spheroids treated with 10, 20 μg/ml of AE for 48 h d) Graphical representation of the decrease in A549 spheroid area when treated with 10 and 20 μg/ml of AE for 48 h. All data are shown as the mean ± SD from three replicate measurements.

3.2. Aqueous and organic extract of O. salina reduced the spheroid area in A549 cells

The observed cytotoxicity induced by *O. salina* extracts on A549 and SKOV-3 cells prompted us to explore the anticancer potential of these extracts on cancer spheroids. Cancer spheroids are known to mimic the architect of tumor microenvironment more accurately than the 2D cultures. The spheroids are characterized by a hypoxic core containing quiescent cells and an outer proliferating zone. The complexity inherent in the 3D spheroid culture system makes it less prone to nonspecific activities, thereby enhancing the likelihood of discovering potent lead compounds. In the present study spheroids formed with A549 and SKOV-3 cells were treated with 10 and 20 μg/ml concentrations of MCE or AE of *O. salina*. After the treatment (72 h for MCE and 48 h for AE), the area of the spheroids formed by A549 cells in each well were determined. The control cells recorded a 6.4 and 9.5 fold increased spheroid area as compared to 10 and 20 μg/ml MCE treated cells respectively (Fig. 2 a, b). Similarly, 10 and 20 μg/ml of AE recorded 5.01 and 7.9 folds decrease spheroid area as compared to respective untreated control (Fig. 2 c, d). However, the spheroids formed by SKOV-3 did not show significant change in spheroid area even after 72 h of AE or MCE treatment with respect to control cells (Supplementary Fig. 2 a, b, c, d). It is important to note that without demonstrating activity in spheroid models, the anticancer potential of these extracts cannot be fully translated to more complex biological systems. As SKOV-3 spheroids were not affected by MCE or AE, all further experiments were conducted with A549 cells.

3.3. MCE and AE of O. salina resulted in the collapse of cytoskeleton in A549 cells

Alterations in the morphology of epithelial cells can result in cell death and detachment. Keratins and actins are intracellular dynamic proteins which provide structural support to the cells [20]. During apoptosis, keratin 18 is reorganized and results in loss of mechanical stability leading to final collapse of the cytoskeleton in epithelial cells. Also, actin is an evolutionarily conserved 42-kDa protein that is essential for the maintenance of cellular morphology and cytoskeleton architecture in epithelial cells [21]. Increasing evidences pointed towards the reorganization of actin cytoskeleton as one of the manifestations of cell shape change and apoptosis [22]. Microscopic data showing MCE and AE-induced change in cell morphology encouraged us to look into the status of these two proteins F-actin and cytokeratin-18 involved in cytoskeleton reorganization. The status of cytoskeletal elements (actin and CK-18) upon change in cell morphology was evaluated by immunofluorescence. Data revealed that A549 cells cultured in absence of MCE or AE maintained the normal actin and CK-18 structure. Staining for CK-18 revealed that MCE and AE treatment (10 μg/ml) for 24 h showed distinct change in CK-18 structure. When the cells were stained for F-actin distinct change in the pattern of actin filaments was observable with 10 μg/ml of AE and MCE for 24 h and 48 h respectively (Fig. 3 a, b). Interestingly, 10 μg/ml of MCE does not show any remarkable change in actin structure of A549 cells after 24 h. In case of MCE the initial change in CK-18 at 24 h might be an early response which could set off a cascade of cellular responses that could lead to actin degradation and complete collapse of cytoskeleton at a later time point of 48 h. However, for AE at 24 h changes in both actin and CK-18 takes place hinting at the greater efficacy of AE than MCE.

3.4. MCE and AE from O. salina induced apoptosis and suppressed cell proliferation in A549 NSCLC cells

Apoptosis, a programmed cell death mechanism inherent in multicellular organisms, plays a crucial role in maintaining cellular

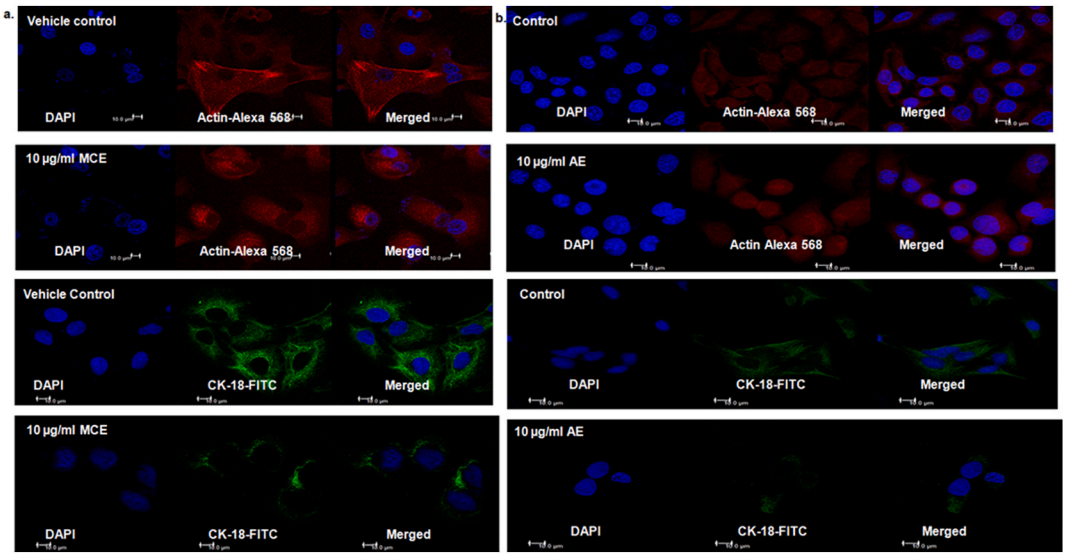

Fig. 3. Effect of *O. salina* extracts on actin and CK-18 in A549 cells. a) Representative images of actin Alexa 568 and CK-18 FITC labeled A549 cells treated with MCE b) Representative images of actin Alexa 568 and CK-18 FITC labeled A549 cells treated with AE.

balance. Dysregulation of the apoptosis signaling pathway is linked to a spectrum of diseases, including cancer. To check whether MCE and AE from *O. salina* could induce apoptosis in A549 cells, we performed AnnexinV/PI staining. Flow cytometry analysis revealed that control cells exhibited 7.35 % of early (annexin V+/PI−) and late (annexin V+/PI+) apoptotic cells, while MCE-treated cells at a concentration of 10 μg/ml showed a significant increase to 28.45 % (Fig. 4 a, b). Moreover, AE treatment at the same concentration resulted in a significant rise in the percentage of early and late apoptotic cells from 9.05 % in the control to 52.3 % in the AE-treated samples (Fig. 4 c, d).

From MTT data it was established that extracts from *O. salina*, specifically MCE and AE, exhibited a dose-dependent decrease in A549 cell viability (Fig. 1 a, b). To substantiate these findings, we conducted a BrdU cell proliferation assay on A549 cells treated with MCE and AE. The BrdU positive cells were detected by using anti-BrdU antibody and quantified by measuring the absorbance at 450 nm. The outcomes demonstrated that concentrations of 20, 50, and 100 μg/ml for both MCE and AE resulted in a significant decrease in cell proliferation compared to their respective controls, as indicated by reduced absorbance at 450 nm (Fig. 4 e, f). These data collectively suggested that both aqueous and organic extracts of *O. salina* at a concentration of 20 μg/ml and higher significantly inhibited proliferation and enhanced apoptosis in A549 cells.

3.5. MCE and AE from O. salina inhibited cell migration and invasion in A549 cells

Wound healing assay was conducted to examine whether *O. salina* extracts could inhibit the motility of the A549 cells. Our result showed that compared to control, MCE treated cells showed significant reduction of cell migration in A549 cells as evident from the reduced percentage of wound closure in MCE treated cells. The percentage of wound closure in the vehicle control cells corresponding to 2.5 μg/ml MCE treatment after 24 h was 79.35 %, whereas in 2.5 μg/ml of MCE treated cells the percentage was 13.26 %. For 5 μg/ml of MCE treatment, the percentage of wound closure after 24 h was 8.90 % while for the corresponding vehicle control it was 78.47

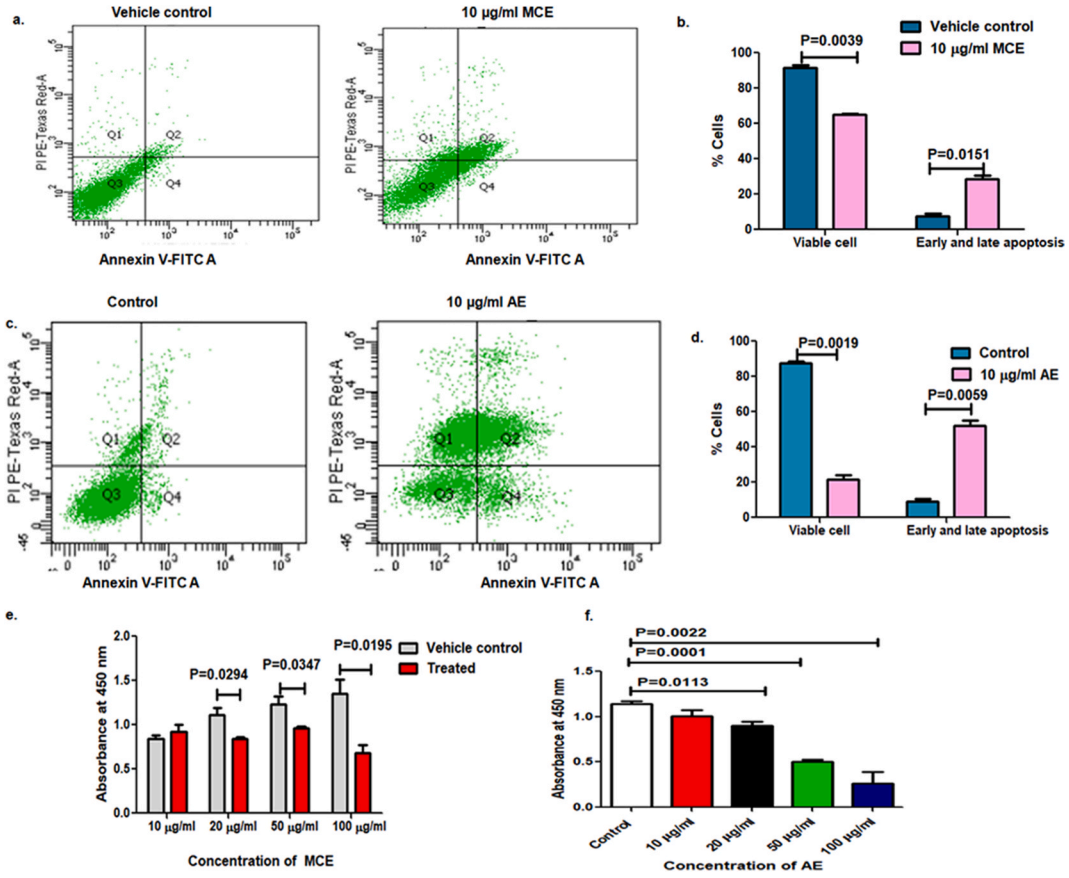

Fig. 4. Apoptosis induced in A549 cells by *O. salina* extracts. a) A549 cells were incubated with 10 μg/ml of MCE for 24 h followed by staining with annexin V/PI. The Q3 quadrant (annexin V−/PI−), Q4 quadrant (annexin V+/PI−) and Q2 quadrant (annexin V+/PI+) indicate the percentage of normal cells, early apoptosis and late apoptosis, respectively, b) Graphical representation of the percentage of viable and apoptotic cells in 10 μg/ml MCE treated and vehicle control groups, c) A549 cells were incubated with 10 μg/ml of AE for 24 h followed by staining with annexin V/PI, d) Graphical representation of the percentage of viable and apoptotic cells in 10 μg/ml AE treated and control groups, e) and f) Bar graph representing the absorbance of BrdU positive cells treated with MCE and AE respectively. All data are shown as the mean ± SD from three replicate measurements.

% (Fig. 5 a and b). Similar wound closure activity was displayed by AE. The control cells show a wound closure of 89.44 % after 24 h, whereas 2.5 and 5 μg/ml of AE treated cells the percentage of wound closure reduced to 11.28 % and 5.06 % respectively (Fig. 5 c, d). This indicated that both MCE and AE significantly suppressed the cell migration in A549 lung cancer cells.

We also measured the effect of *O. salina* extracts on the invasive ability of A549 cells. Cells treated with 10 and 20 μg/ml of MCE or AE showed significant ($P < 0.05$) reduction of invasive capacity of A549 cells as evident from both microscopic images (Fig. 5 e) as well as OD values of the stained cells that have invaded through the matrigel to the lower surface of the transwell insert (Fig. 5 f, g).

3.6. Transcriptomics analysis of A549 cells treated with MCE and AE of O. salina

To delve into the mechanistic details of anticancer and antimetastatic effect of different *O. salina* extracts RNA-sequencing was performed. Based on phenotypic experiments, RNA-sequencing was performed with A549 cells treated with 10 μg/ml of AE or MCE or their respective control for different time points (24 h for MCE and 8 h for AE). An early time point for AE treated cells were taken for RNA-sequencing experiment as morphology change in AE treated cells were seen at 24 h as compared to 48 h in case of MCE treated cells.

High-throughput sequencing was conducted for the systematic analysis of gene expressions in A549 cells with or without exposure to *O. salina* extracts. A549 cells treated with 10 μg/ml of MCE for 24 h displayed an altered global transcriptome profile with 434 differentially expressed genes (with $P < 0.05$ and $\log_2$fold change >1) among which, 356 genes were up-regulated and 78 genes were down-regulated as compared to vehicle treated control. The degree of expression change of these DEGs between the two samples is shown as a volcano plot in Fig. 6 a. Functional annotation of the DEGs showed that these genes were distributed into three main functional biological categories: biological process, cellular component, and molecular function. Significant biological processes mainly included angiogenesis, cell adhesion, apoptosis, lipid transport and phagocytosis. Cellular component included cell projection, cytoplasm, cytoskeleton, cell junction, membrane, cell membrane, basement membrane, sarcoplasmic reticulum, cytoplasmic vesicle and golgi apparatus. Molecular function included guanine-nucleotide releasing factor, kinase, GTPase activation, calmodulin binding, serine threonine protein kinase, transferase, cytokine, ligase, protein phosphatase, integrin and protein phosphatase Fig. 6 b. Analysis using the Kyoto Encyclopedia of Genes and Genomes (KEGG) indicated that the majority of the perturbed genes were linked to pathways related to Rap1 signaling, p53 signaling, pathways in cancer, focal adhesion, IL-17 signaling pathway (Table 1). These findings indicated that these signaling might be critical in induction of apoptosis in A549 cells by MCE.

Similar analysis with A549 cells treated with 10 μg/ml of AE for 8 h indicated that 263 genes were differentially regulated in AE treated cell as compared to the control sample. Among these genes 12 are up-regulated and 251 are down-regulated (Fig. 6 c). Functional annotation using DAVID indicated three main functional categories: biological process, cellular component, and molecular function. Biological processes included apoptosis, angiogenesis and t-RNA processing. The GO terms included in the cellular

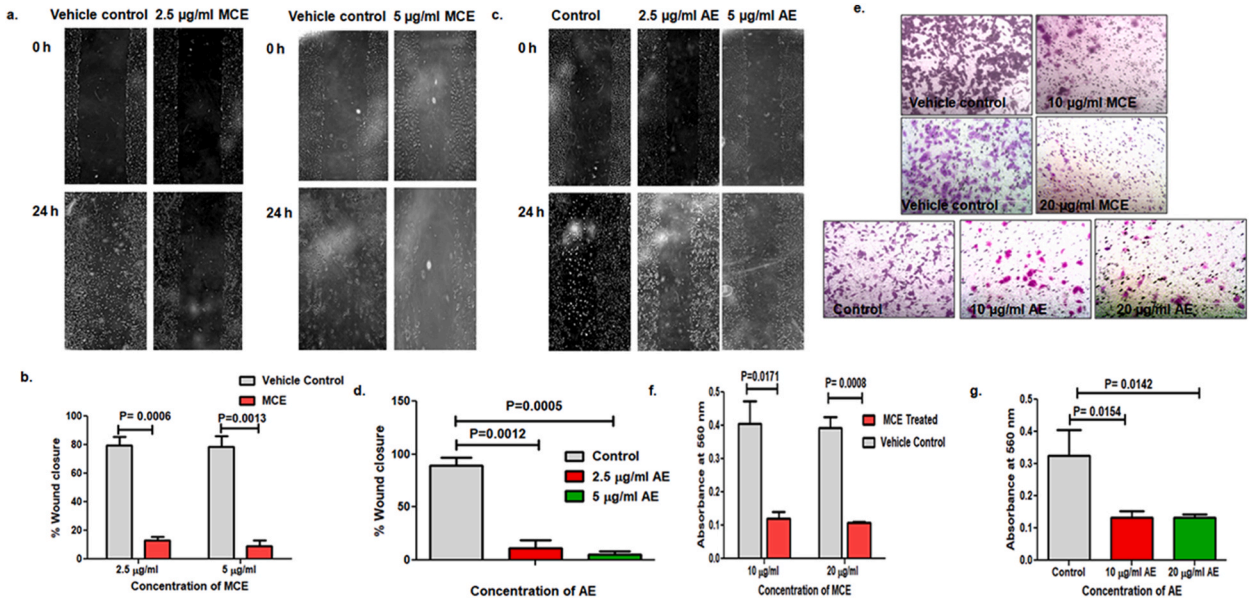

Fig. 5. Inhibition of cell migration and invasion in A549 cell by *O. salina* extracts. a) Representative image of wound closure in A549 cells treated with 2.5 and 5 μg/ml MCE at 0 h and 24 h time points, b) Graphical representation of percentage of wound closure in MCE treated A549 cells at 0 h and 24 h, c) Representative image of wound closure in A549 cells treated with 2.5 and 5 μg/ml AE at 0 h and 24 h time points, d) Graphical representation of percentage of wound closure in AE treated A549 cells at 0 h and 24 h, e) Representative image of the MCE and AE treated cells invaded to the lower surface of the transwell insert, f) and g) Quantification of the MCE and AE treated A549 cells invaded to the lower surface of transwell insert by measuring the absorbance of the stained cell at 560 nm. All data are shown as the mean ± SD from three independent measurements.

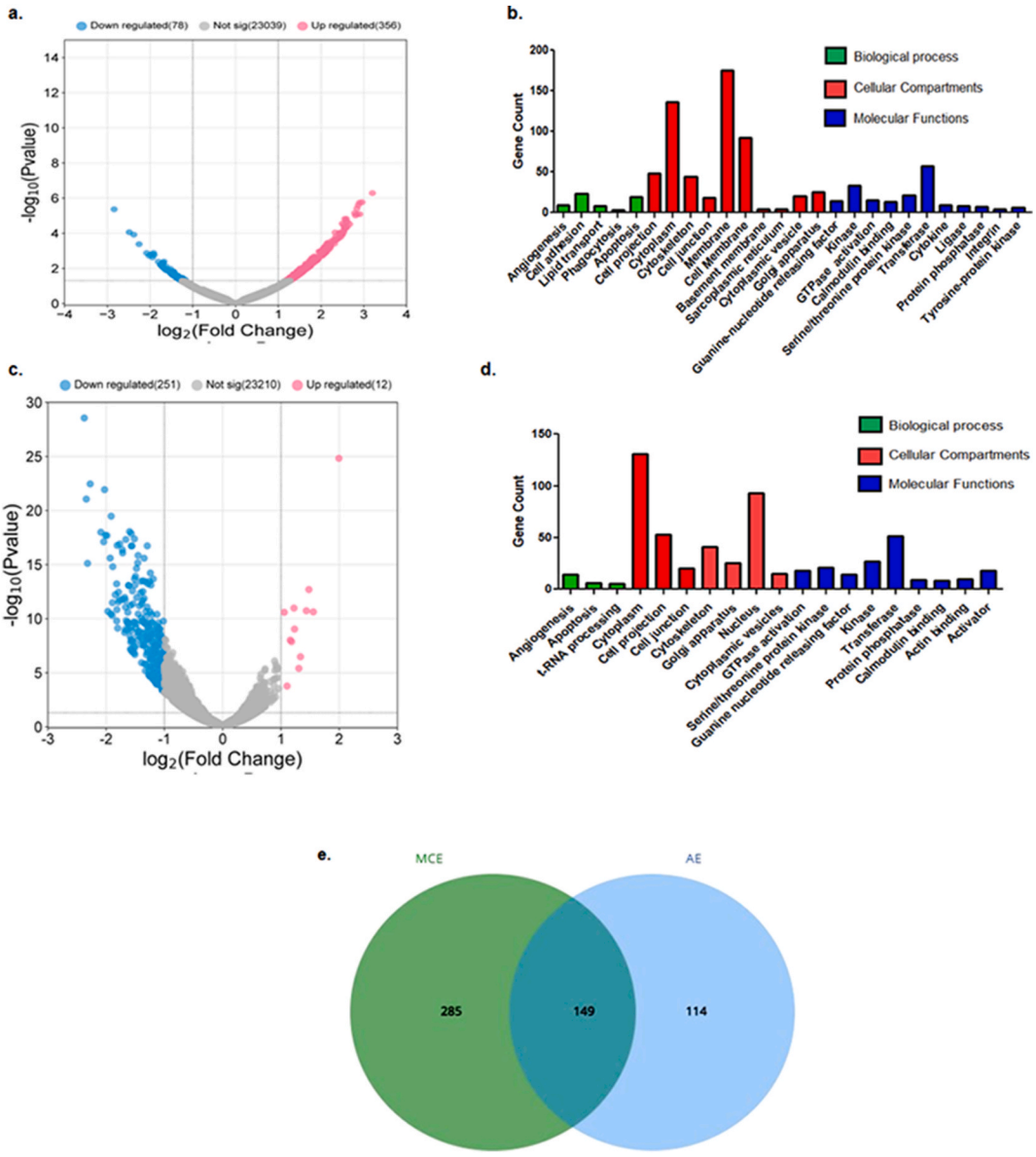

Fig. 6. Transcriptomics analysis of A549 cells treated with *O. salina* extracts. a) Volcano plot of the identified DEGs between control A549 cells and A549 cells treated with 10 μg/ml MCE for 24 h, b) GO functional enrichment analysis of the DEGs between control A549 cells and A549 cells treated with 10 μg/ml MCE for 24 h, c) Volcano plot of the identified DEGs between control A549 cells and A549 cells treated with 10 μg/ml AE for 8 h, d) GO functional enrichment analysis of the DEGs between control A549 cells and A549 cells treated with 10 μg/ml AE for 8 h, e) Venn diagram showing number of overlapping genes between MCE and AE treatment.

component are cytoplasm, cell projection, cell junction, cytoskeleton, golgi apparatus, nucleus and cytoplasmic vesicles. Molecular function included GTPase activation, guanine nucleotide releasing factor, kinase, serine/threonine protein kinase, transferase, protein phosphatase, calmodulin binding, actin binding and activator (Fig. 6 d). Kyoto Encyclopedia of Genes (KEGG) analysis revealed that most of the regulated genes were associated with pathways involving Rap1 signaling, p53 signaling, MAPK (mitogen activated protein kinase) signaling, notch signaling, Wnt signaling (Table 1). These results hinted at the involvement of these pathways in AE mediated cell apoptosis. In addition, the comparative analysis of gene expression profiles in MCE and AE-treated A549 cells revealed a total of 149 overlapping DEGs between the two treatment modes (Fig. 6 e). This comprehensive genomic exploration highlighted both shared and distinct regulatory responses, underscoring the nuanced impact of MCE and AE on the cellular transcriptome.

Table 1
KEGG categories of DEGs in each pathway shown with the total number of annotated genes in these pathways for MCE-treated and AE-treated cells.

Term	Gene Count for MCE Treatment\1	Gene Count for AE Treatment\1
Rap1 signaling pathway	12	15
P53 signaling pathway	6	5
Pathways in cancer	20	–
IL-17 pathway	6	–
Focal adhesion	12	–
MAPK signaling pathway	–	9
Notch signaling pathway	–	4
Wnt signaling pathway	–	6

3.7. *Characterization of the bioactive components in AE and MCE of O. salina*

AE (5 mg/ml) on HPLC analysis displayed two major and four minor peaks at 620 nm (Fig. 7 a, b) (Lemos et al., 2020). All the six peaks have displayed similar UV absorption spectrum having UV absorption maxima at 277, 345 and 616 nm indicating that the extract contains phycocyanins (Fig. 7 c). FT-IR spectrum of AE displayed absorbance peaks at 3282, 2927, 1645, 1542, 1408, 1087, 1039, 994, 703 and 623 cm $^{-1}$ (Fig. 7 e). The extract generated a complex NMR spectrum displaying the signals in the range of δ H 0.86–8.28 (Fig. 7 f). However, no peaks in HPLC was observable for MCE at a concentration of 5 mg/ml. At 10 mg/ml MCE displayed a very few minor peaks in HPLC which are different from those observed for AE (Fig. 7 d). This could be attributed to the lower concentration of compounds in MCE. Hence to decipher the metabolites in MCE we performed LC-MS/MS analysis (Supplementary file 5). Comparisons of the mass spectral peaks with the molecular formula database of more than 2100 cyanobacterial metabolites, CyanoMetDB [23] allowed the prospective annotation of 11 of those metabolites (Table 2). These compounds included tumonoic acid, mooreamide A, ambiguine I isonitrile, mirabilene A isonitrile, tricholide A, ypaomide C, ambiguine E isonitrile, fischambiguine B, cybastacine A, muscoride A, carbamidocyclophane R.

4. Discussion

Cyanobacterial metabolites exhibit significant promise in clinical applications [24] due to their high chemical diversity and biodiversity [25]. Despite this potential, the bioactive capabilities of the majority of strains remain largely unexplored. In the present study, we employed a combination of in vitro anticancer assays and chemical methods of metabolite characterization of a previously

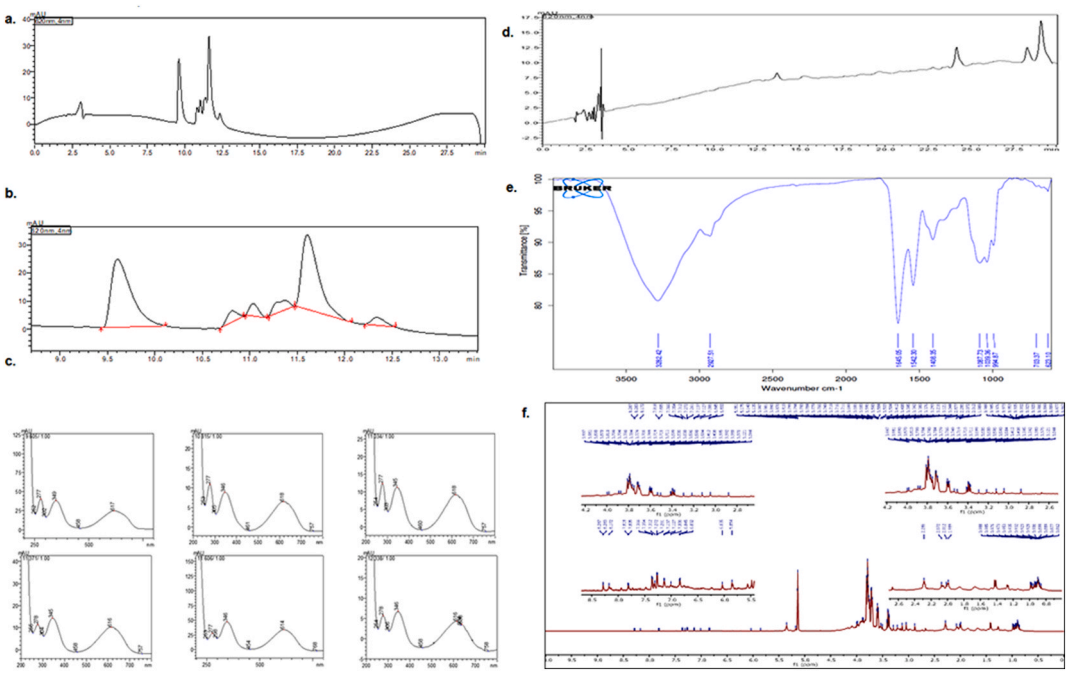

Fig. 7. Characterization of bioactive metabolites in AE. a) HPLC chromatogram of AE at 620 nm, b) Expansion of HPLC chromatogram 9–13 min, c) UV absorption spectrum of individual peaks obtained using PDA detector, d) HPLC chromatogram of MCE at 620 nm, e) IR spectrum of AE, f) 1 H NMR spectrum of AE.

Table 2
Annotation of the putative metabolites with their *m/z* values present in MCE of *O. salina* by comparing with CyanoMetDB database.

Metabolite	Experimental *m/z*	Database *m/z*
Tumonoic acid E	326.23	326.23258460000005
Mooreamide A	390.3	390.3002703
Ambiguine I isonitrile	403.24	403.2380043
Mirabilene A isonitrile	408.31	408.310835
Tricholide A	408.31	408.310835
Ypaoamide C	425.22	425.2201614
Ambiguine E isonitrile	437.2	437.19903200000005
Fischambiguine B	437.2	437.19903200000005
Cybastacine A	477.34	477.34353210000006
Muscoride A	513.31	513.3071466
Carbamidocyclophane R	706.33	706.331292

unexplored strain of marine cyanobacterium *O. salina*. The objective was to evaluate the anticancer potential of organic and aqueous extracts obtained from *O. salina* and also to elucidate the specific metabolites present in the extracts with anticancer activities.

Metabolite profiling serves as a valuable tool for the selection of promising fractions, allowing for the assessment of their chemical profiles. Comparison of the mass spectral peaks obtained for MCE with that of the cyanobacterial metabolite database CyanoMetDB hinted at the presence of 11 compounds. Among these compounds ambiguine I isonitrile has been reported to induce caspase-independent cytotoxicity and cell death in MCF-7 breast cancer cell line [26]. Additionally, ambiguine E isonitrile, carbamidocyclophane, mirabilene isonitrile also display cytotoxic effect [27,28] in different cell lines. Therefore, the anticancer activity observed in MCE could be attributed to the presence of these compounds in MCE.

The HPLC analysis of the aqueous extract (AE) revealed the presence of six distinct peaks, prominently observed at ~620 nm. These peaks signify the intricate composition of phycocyanins, water-soluble phycobiliproteins characterized by tetrapyrrole groups, which are responsible for light absorbance. A typical absorption at ~620 nm indicates that the extract contains a group of phycocyanins which is distinctly different from the phytoerythrin and allophycocyanin which displays the absorption maxima at 565 and 650 nm, respectively [29,30]. FT- IR spectrum of the extract displayed an intense absorbance band at 1645 cm $^{-1}$ indicated the presence of amide linkage (-C=O stretching) [31,32]. The NMR spectroscopy in particular helps in determining the chemical structures of any given compound, as the protons in the molecule generate distinct signals. However, in case of mixture of compounds and specially mixture of phycocyanin type of proteins containing tertrapyrrole groups the NMR spectrum displays a complex peak patterns due to the overlapping. In spite of that these complex NMR could be utilized to tentatively ascertain the presence various type of protons. In present case also, the extract generated a complex NMR spectrum in the range of δ H 0.86–8.28. This indicates the presence of protons corresponding to both aliphatic and aromatic regions. Of these, the signals at δ H 2.0–3.5 could be attributed to the presence of aliphatic methyl and methylene groups. Proton signals in the range of δ H 5.1–6.0 indicates the presence of protons associated with olefinic bonds. Proton signals appearing in other ranges could be associated with the different parts of the proteins [33,34]. Since it is reported earlier that the phycocyanin C is composed of two different subunits (α and β) are the two distinct peaks shown in HPLC analysis [30]. In our case also the extract shows two major peaks with other minor peaks suggested a detailed investigation for their structure determination.

In a prior investigation conducted in our laboratory, it was observed that both AE and MCE exhibited dose dependent cytotoxic effects on A549 and SKOV-3 cells as determined through the MTT assay. The lowest IC50 value was observed for A549 cells. In addition, MCE and AE could not induce spheroid disintegration in SKOV-3 cells. Since spheroids accurately recapitulate the in vivo tumor microenvironment, they are invaluable for assessing the true therapeutic potential and effectiveness of anticancer agents. Hence further experiments were not proceeded with SKOV-3 cells. In the present study we screened an aqueous and organic extract of *O. salina* to identify possible hits with apoptosis-inducing activity in A549 lung cancer cells. In this context, it is important to mention that the MTT assay may inherently underestimate the actual effectiveness of anticancer drugs when assessing in terms of cytotoxicity and apoptosis. Hence in the present study, the induction of apoptosis by *O. salina* extracts was confirmed by the flow cytometric analysis of cells stained with Annexin V-FITC and PI. Here, it is noteworthy to highlight that a comparable alteration in morphology as well as induction of apoptosis was previously noted in A549 cells upon exposure to phycocyanin [35]. Considering that phycocyanin is identified as a constituent of AE, it is plausible to attribute the observed morphological changes and apoptosis in A549 cells to the presence of phycocyanin in AE. Furthermore, the morphological alterations in A549 cells induced by *O. salina* extracts (both MCE and AE) not only suggest that the cell death occurs by apoptosis but also indicated that these extracts induced collapse of the cytoskeleton and decreased cell-cell adhesion. We also evaluated the anticancer potential of *O. salina* extracts in 3D spheroid model as spheroids exhibit greater resistance to anticancer drugs compared to the same cells grown as monolayer cell cultures. The observed resistance of spheroids to various treatment methods could be due to the heterogeneity in the uptake of certain drugs. Hence spheroid model enables the evaluation of the drug penetration properties. Our study shows that *O. salina* extracts at concentrations of 10 and 20 μg/ml could significantly reduce the spheroid area in A549 cells. Taken together these data suggested that both AE and MCE from *O. salina* could significantly show anticancer activities in 2D as well as 3D cell culture model. However, MCE required a longer time to induce spheroid disintegration and morphological changes. This could be explained by our HPLC analysis, which showed no detectable peaks for MCE at a lower concentration (5 mg/ml), unlike AE which displayed distinct peaks at this concentration. When HPLC was performed with

MCE at a higher concentration (10 mg/ml) we could see a few peaks. However, the peak patterns of the two extracts are completely different and no peaks for phycocyanin were observed in the MCE at 620 nm (Fig. 7 d) for the samples analyzed using the same HPLC method. This suggested that the concentrations of individual metabolites in MCE were lower than those in AE. Consequently, the lower efficacy of MCE compared to AE could be due to these reduced metabolite concentrations.

Transcriptomics analysis has been recognized as a gold standard for identifying genetic signatures and elucidating biological processes linked to human diseases, including cancer [36]. To better elucidate the anticancer effect of *O. salina* extracts at the molecular level, we used RNA-Seq analysis to determine changes in gene expression in A549 cells treated with *O. salina* extracts. As seen in phenotypic experiments, the distinct morphology change was observed in the case of 10 μg/ml AE-treated cells at an early time point (24 h) as compared to those in 10 μg/ml MCE-treated cells (48 h). Therefore, an early time point (8 h) was chosen in case of AE-treated A549 cells for transcriptomics analysis. Whereas for MCE a late time point of 24 h was chosen. The morphology changes at a late time point (48 h) in MCE treated cells as compared to AE treatment might be linked to the lower concentration of metabolites in MCE as compared to AE. In MCE treated cells total number of DEGs was 434. Functional annotation of these DEGs indicated that these genes were associated with biological processes like apoptosis, phagocytosis, cell adhesion etc. This evidence aligned with our experimental findings that MCE in A549 cells lead to cellular apoptosis and loss of cell-cell adhesion. KEGG analysis indicated that the perturbed genes in MCE treated cells are linked to cancer-related pathways including Rap1 signaling, p53 signaling, focal adhesion, IL-17 signaling pathway. Rap1, a member of the Ras-like small GTP binding protein family, is associated with malignancy in NSCLC [37]. The Ras family regulates a spectrum of both benign and malignant biological processes, including but not limited to cell adhesion, growth, apoptosis, and migration and invasion [38]. Kan et al. [39], showed that cell invasion and metastasis in A549 cells could be regulated by inhibition of Rap1 signaling. Another signaling pathway that has been perturbed by MCE in A549 cells is the IL-17 signaling pathway. Lung cancer has been an inflammation-associated carcinoma and IL-17 plays an important role in chronic inflammation associated tumors. A study by Tania et al. [40], showed that IL-17 could promote the migration and invasion of A549 cells via the NF-κB pathway. Consequently, it is plausible to hypothesize that the modulation of Rap1 and IL-17 signaling pathways may contribute to MCE-induced apoptosis, proliferation inhibition, and the restraint of invasion and migration in A549 cells. Furthermore, KEGG analysis of the perturbed genes in AE treated cells also indicated the participation of Rap1 and p53 signaling pathway similar to that in MCE-treated cells. In addition, mitogen activated protein kinase (MAPK), notch and Wnt signaling pathways are also involved in AE-mediated antitumor response. Wnt and notch expression is associated with epithelial mesenchymal transition (EMT) and poor prognosis in NSCLC patients [41,42]. Notch signaling plays an important role in proliferation, adhesion, apoptosis, migration, angiogenesis, EMT, and stem cell maintenance [43]. Given that phycocyanin has been identified as a potential bioactive component of AE, it is plausible that the perturbation of these pathways could be mediated by phycocyanin. Moreover, comparative analysis of gene expression profiles in MCE and AE-treated cells unveiled 149 overlapping DEGs. Also, MCE and AE treatment led to the identification of 285 and 114 unique DEGs for MCE and AE treatment modes respectively. This detailed examination underscored the intricate regulatory impact of MCE and AE on the cellular transcriptome, showcasing both shared and specific gene expression responses although the time points were different for MCE and AE.

Taken together, our study indicated that metabolites from *O. salina* dose-dependently induced cytotoxicity, inhibited cell proliferation, and altered cell morphology in A549 cells with a minimal concentration of 10 μg/ml active against A549 cell line. These results were further confirmed by apoptosis assay and immunocytochemistry where the minimal active concentration was used. Additionally, *O. salina* metabolites demonstrated significant anti-migratory activity at much lower doses of 2.5 and 5 μg/ml, as evidenced by cell migration assay. These findings suggested that different biological activities, such as anti-proliferative and anti-migratory effects, are dose-dependent when using *O. salina* metabolites, indicating the need for precise dosing to achieve desired therapeutic outcomes.

5. Conclusion

Recently, marine organisms have gained prominence as a promising reservoir of potent anticancer drugs, showcasing efficacy against both newly identified and drug-resistant cancer types. To the best of our knowledge, this study is the first to demonstrate the anticancer and anti-metastatic activity of a previously unexplored strain of marine cyanobacterium, *O. salina*. In this study, we also explored the probable metabolites in the aqueous (AE) and methanol chloroform (MCE) extracts of *O. salina*. Our results demonstrated that both AE and MCE possess significant anti-cancer effects, effectively inducing apoptosis and inhibiting cell proliferation in A549 cells. Notably, the anticancer efficacy of AE and MCE was confirmed in 3D spheroid models. Importantly, the concentrations at which AE and MCE exhibit cytotoxic effects on cancer cells do not induce significant toxicity or alter the morphology in normal human embryonic kidney cells HEK293 (Supplementary Fig. 1 a, b, c, d). This therapeutic window highlights the potential for these extracts to be developed into targeted treatment strategies for cancer therapy. The encouraging outcomes of this study, coupled with the simplicity and cost-effectiveness of the culturing and extraction techniques, emphasize the necessity to isolate and explore the therapeutic potential of specific metabolites in *O. salina* and their underlying mechanisms of action. However, further in vivo studies are necessary to evaluate the anti-cancer efficacy and toxicity of the *O. salina* MCE and AE in a xenograft model. These studies are essential before considering their potential development and application as an alternative treatment for lung or other cancers.

Funding

The project is funded by CSIR-IICB (grant no. CSIR-P07), DBT BIC (grant no. BT/PR40137/BTIS/137/35/2022), Department of Health Research (grant no. 12013/04/2021-HR) and DBT NNP (grant no. BT/PR40243/BTIS/137/75/2023). BD and AP are recipients of DHR WOS Fellowship and UGC Fellowship respectively. SD is supported by ICMR fellowship. AM was funded by DBT BIC scheme.

YD is a recipient of CSIR fellowship.

Data availability

All the raw reads of RNA-sequencing experiments are available at SRA-NCBI. SRA accession no. are SRR27437186 and SRR27437187.

CRediT authorship contribution statement

Bornita Das: Writing – review & editing, Writing – original draft, Visualization, Validation, Resources, Methodology, Investigation, Formal analysis, Data curation, Conceptualization. **Asharani Prusty:** Methodology, Investigation, Formal analysis, Data curation. **Subhajeet Dutta:** Software, Methodology, Formal analysis. **Aditi Maulik:** Software, Methodology, Formal analysis. **Yogita Dahat:** Methodology, Investigation, Formal analysis, Data curation. **Deepak Kumar:** Visualization, Validation, Formal analysis, Data curation. **Sucheta Tripathy:** Writing – review & editing, Supervision, Resources, Funding acquisition, Conceptualization.

Declaration of competing interest

The authors declare the following financial interests/personal relationships which may be considered as potential competing interests: None If there are other authors, they declare that they have no known competing financial interests or personal relationships that could have appeared to influence the work reported in this paper.

Acknowledgements

The authors would like to acknowledge Dr. Rupasri Ain, chief scientist, Cell Biology and Physiology Division, CSIR-IICB for her valuable suggestions and Dr. Nahid Ali, J. C. Bose Fellow, INSA Emeritus Scientist, CSIR-IICB for providing cell culture facilities.

Appendix A. Supplementary data

Supplementary data to this article can be found online at https://doi.org/10.1016/j.heliyon.2024.e36048.

References

[1] A. Karthikeyan, A. Joseph, B.G. Nair, Promising bioactive compounds from the marine environment and their potential effects on various diseases, J. Genet. Eng. Biotechnol. 20 (1) (2022) 1–38.
[2] J. Demay, et al., Natural products from cyanobacteria: focus on beneficial activities, Mar. Drugs 17 (6) (2019) 320.
[3] A.C. Jones, et al., The unique mechanistic transformations involved in the biosynthesis of modular natural products from marine cyanobacteria, Nat. Prod. Rep. 27 (7) (2010) 1048–1065.
[4] D. Dhakal, et al., Heterologous production of cyanobacterial compounds, J. Ind. Microbiol. Biotechnol. 48 (3–4) (2021).
[5] K. Kleigrewe, et al., Unique marine derived cyanobacterial biosynthetic genes for chemical diversity, Nat. Prod. Rep. 33 (2) (2016) 348–364.
[6] A. Mondal, et al., Marine cyanobacteria and microalgae metabolites—a rich source of potential anticancer drugs, Mar. Drugs 18 (9) (2020) 476.
[7] S.A.A. Shah, et al., Structural diversity, biological properties and applications of natural products from cyanobacteria. A review, Mar. Drugs 15 (11) (2017) 354.
[8] B. Robles-Bañuelos, et al., Marine cyanobacteria as sources of lead anticancer compounds: a review of families of metabolites with cytotoxic, antiproliferative, and antineoplastic effects, Molecules 27 (15) (2022) 4814.
[9] S. Kato, et al., Challenges and perspective of drug repurposing strategies in early phase clinical trials, Oncoscience 2 (6) (2015) 576.
[10] R.K. Singh, et al., Cyanobacteria: an emerging source for drug discovery, The Journal of antibiotics 64 (6) (2011) 401–412.
[11] A. Bouyahya, et al., Bioactive substances of cyanobacteria and microalgae: sources, metabolism, and anticancer mechanism insights, Biomed. Pharmacother. 170 (2024) 115989.
[12] C.-C. Liang, A.Y. Park, J.-L. Guan, In vitro scratch assay: a convenient and inexpensive method for analysis of cell migration in vitro, Nat. Protoc. 2 (2) (2007) 329–333.
[13] A. Suarez-Arnedo, et al., An image J plugin for the high throughput image analysis of in vitro scratch wound healing assays, PLoS One 15 (7) (2020) e0232565.
[14] B. Bushnell, BBMap: a Fast, Accurate, Splice-Aware Aligner, Lawrence Berkeley National Lab.(LBNL), Berkeley, CA (United States), 2014.
[15] B. Bioinformatics, FastQC: a Quality Control Tool for High Throughput Sequence Data, Babraham Institute, Cambridge, UK, 2011.
[16] A. Dobin, et al., STAR: ultrafast universal RNA-seq aligner, Bioinformatics 29 (1) (2013) 15–21.
[17] Y. Liao, G.K. Smyth, W. Shi, featureCounts: an efficient general purpose program for assigning sequence reads to genomic features, Bioinformatics 30 (7) (2014) 923–930.
[18] D.W. Huang, B.T. Sherman, R.A. Lempicki, Systematic and integrative analysis of large gene lists using DAVID bioinformatics resources, Nat. Protoc. 4 (1) (2009) 44–57.
[19] B.T. Sherman, et al., DAVID: a web server for functional enrichment analysis and functional annotation of gene lists (2021 update), Nucleic acids research 50 (W1) (2022) W216–W221.
[20] B. Schutte, et al., Keratin 8/18 breakdown and reorganization during apoptosis, Experimental cell research 297 (1) (2004) 11–26.
[21] E. Papakonstanti, C. Stournaras, Cell responses regulated by early reorganization of actin cytoskeleton, FEBS Lett. 582 (14) (2008) 2120–2127.
[22] S.R. White, et al., Initiation of apoptosis by actin cytoskeletal derangement in human airway epithelial cells, Am. J. Respir. Cell Mol. Biol. 24 (3) (2001) 282–294.
[23] M.R. Jones, et al., CyanoMetDB, a comprehensive public database of secondary metabolites from cyanobacteria, Water Res. 196 (2021) 117017.
[24] A.R. Carroll, et al., Marine natural products, Nat. Prod. Rep. 36 (1) (2019) 122–173.
[25] E. Dittmann, et al., Natural product biosynthetic diversity and comparative genomics of the cyanobacteria, Trends Microbiol. 23 (10) (2015) 642–652.

[26] U.M. Acuña, et al., Ambiguine I isonitrile from fischerella ambigua induces caspase-independent cell death in MCF-7 hormone dependent breast cancer cells, Int. J. Cancer Res. 49 (1) (2015) 1655–1662.
[27] S. Mo, et al., Antimicrobial ambiguine isonitriles from the cyanobacterium fischerella ambigua, Journal of Natural Products 72 (5) (2009) 894–899.
[28] H.T. Bui, et al., Carbamidocyclophanes A– E, chlorinated paracyclophanes with cytotoxic and antibiotic activity from the Vietnamese cyanobacterium nostoc sp, Journal of natural products 70 (4) (2007) 499–503.
[29] L. Bogorad, Phycobiliproteins and complementary chromatic adaptation, Annu. Rev. Plant Physiol. 26 (1) (1975) 369–401.
[30] D. Kumar, et al., Extraction and purification of C-phycocyanin from Spirulina platensis (CCC540), Indian J. Plant Physiol. 19 (2014) 184–188.
[31] P.V.F. Lemos, et al., Preparation and characterization of C-phycocyanin coated with STMP/STPP cross-linked starches from different botanical sources, Int. J. Biol. Macromol. 159 (2020) 739–750.
[32] A. Husain, et al., Physicochemical characterization of C-phycocyanin from Plectonema sp. and elucidation of its bioactive potential through in silico approach, Cellular and Molecular Biology 67 (4) (2021) 68–82.
[33] G. Prabakaran, et al., Extraction and characterization of phycocyanin from Spirulina platensis and evaluation of its anticancer, antidiabetic and antiinflammatory effect, Int. J. Biol. Macromol. 153 (2020) 256–263.
[34] W. Cole, D.J. Chapman, H.W. Siegelman, Structure of phycocyanobilin, J. Am. Chem. Soc. 89 (14) (1967) 3643–3645.
[35] S. Hao, et al., The in vitro anti-tumor activity of phycocyanin against non-small cell lung cancer cells, Mar. Drugs 16 (6) (2018) 178.
[36] S. Supplitt, et al., Current achievements and applications of transcriptomics in personalized cancer medicine, Int. J. Mol. Sci. 22 (3) (2021) 1422.
[37] L. Xiao, et al., Cytoplasmic RAP1 mediates cisplatin resistance of non-small cell lung cancer, Cell Death Dis. 8 (5) (2017) e2803.
[38] O. Maertens, K. Cichowski, An expanding role for RAS GTPase activating proteins (RAS GAPs) in cancer, Adv. Biol. Regul. 55 (2014) 1–14.
[39] J. Kan, et al., He-Chan Pian inhibits the metastasis of non-small cell lung cancer via the miR-205-5p-mediated regulation of the GREM1/Rap1 signaling pathway, Phytomedicine 94 (2022) 153821.
[40] M. Tania, M.A. Khan, J. Fu, Epithelial to mesenchymal transition inducing transcription factors and metastatic cancer, Tumor Biol. 35 (2014) 7335–7342.
[41] B. Das, D. Sinha, Diallyl disulphide suppresses the cannonical Wnt signaling pathway and reverses the fibronectin-induced epithelial mesenchymal transition of A549 lung cancer cells, Food Funct. 10 (1) (2019) 191–202.
[42] T. Menju, H. Date, Lung cancer and epithelial-mesenchymal transition, General Thoracic and Cardiovascular Surgery 69 (2021) 781–789.
[43] V. Kumar, et al., The role of Notch, Hedgehog, and Wnt signaling pathways in the resistance of tumors to anticancer therapies, Front. Cell Dev. Biol. 9 (2021) 650772.